WESTERN LAMPUNG PROBABILISTIC TSUNAMI HAZARD MODEL: INVESTIGATIONS BY AERIAL PHOTOGRAMMETRY AND REMOTE SENSING DATA

Arliandy P. Arbad(1), W. Takeuchi(2), S. Jonathan(3), M. Jamilah (4)
Achmad Ardy(5), Chusna Meimuna (6)

[1] State Polytechnic of Jakarta., Jl. Prof. Dr. G.A Siwabessy, Kampus Baru UI Depok, Indonesia
[2] Institute of Industrial Science, The University of Tokyo, Japan
[3] Dept. of Geomatics Engineering, Institute Technology of Sumatera, Lampung, Indoesia
[4] Dept. of Geodesy Engineering, Diponegoro University, Semarang, Indonesia
[5] Dept. of Agroecotechnology, Lampung University, Lampung, Indonesia
[6] Public Health Department, The University of Indonesia, Depok, Indonesia ore University, 02841

Email: arliandy.pratama@sipil.pnj.ac.id

KEY WORDS: Lampung, Tsunami, Hazard, Photogrammetry, Remote Sensing

ABSTRACT: The series of deadly tsunamis in recent years in Indonesia, such as the extreme events in Aceh-Sumatera Island (2004), Lombok Island (2018), Palu-Sulawesi Island (2018), and most recently in Lampung-Sumatera Island (2018) is a natural disaster destructive power. While earthquakes allow at best several seconds of warning, the time available for issuing a tsunami warning ranges from minutes to many hours. Sumatra Island is one of the areas located in areas prone to the natural disaster, such as earthquake, landslide and tsunami. Sumatra is flanked by two main epicenter Great Sumatran Fault throughout of the Bukit Barisan and two subduction zones both the Indo-Australian Plate and the Eurasian Plate. The aim of this research is how to create a probabilistic model of Tsunami in Western Lampung. Modern technologies in combination with remotely sensed data in GIS environment open a wide field for assisting in Crisis Management. The most important component of any Crisis Management System is a Crisis Preparedness Plan where especially our disciplines of Photogrammetry and Remote Sensing can contribute in many ways. Georeferenced photographs methods to produce a 3D-digital surface model (DSM) of the area and its associated orthophotograph, the method for determining the inundation area and the travel time of a tsunami is used a simple calculation of distance and depth. Furthermore, we investigated the potential landslide in the study area by using SAR Interferometry, simulations of landslide-triggered tsunamis, which could affect coastal localities even following relatively small destabilized volumes.

1. INTRODUCTION

In the past 15 years, many large earthquakes and tsunamis have shaken Indonesia. If sorted from the north, the order is Aceh, Nias, Padang, Bengkulu, Tasikmalaya, Ciamis and Jogja. But if seen in more detail, there are areas where the order is always skipped, namely Lampung and the Sunda Strait. The earthquake in Lampung, which caused by subduction of the Indo-Australian plate against the Eurasian Plate, Semangko Fault, and Faulting of the plate. Moreover, Lampung is hitting by plates tectonic from the two directions, from the south and from the west. The subductions were issued by other faults in the Lampung area. Like the Semangko fault in the west of Lampung, and the Tarahan fault that passes through the city of Bandar Lampung. These faults become a kind of earthquake that deserves caution. One of the large earthquakes had hit Lampung, such as the 1994 Liwa earthquake, M 7. The earthquake originated from the Semangko fault shift. Material density in the oceanic crust (the Indo-Australian Plate) is higher dissolving material on the continental crust (Eurasian Plate) and elements in the continental crust, this condition causes the Indo-Australian Plate to be pushed down the Eurasian Plate. Another disaster is tsunami which caused by the active volcano, Anak Krakatau.

Questions still abound about what caused the tsunami that hit beaches in Lampung in particular at Western Lampung. The local authority confirmed there had been a tsunami but no tectonic activity in the area, and that they suspected the tsunami was caused by an eruption from the volcano, to trigger a tsunami that large, there needs to be a massive landslide that falls into the sea and that requires a large amount of energy, which has not been detected by seismographs in volcanic observation posts.

Furthermore, we have to consider about 13 % of the world's active volcanoes are located in Indonesia. Tectonically, the active volcanoes are the result of a collision between Indian-Australian, Eurasian, and Philippine Plates [Zaennudin, 2010]. One of the most powerful volcano is closely located to Bandar Lampung, the volcano is Mt. Anak Krakatoa. The objective of this study is to model the probabilistic tsunami hazard based on ground deformations monitoring, landslide, and volcano activity. We used InSAR (interferometric SAR) in Western Lampung including Anak Krakatoa super volcano to identify the characteristics and status of volcano, the most commonly technique is used remote sensing method [Lu et al, 2007] and photogrammetry [Dai, F., et al, 2011] to produce a 3D-digital surface model (DSM) of the area and its associated orthophotograph, the method for determining the inundation area and the travel time of a tsunami is used a simple calculation of distance. Photogrammetry and remote sensing has been largely implemented to identify and characterize of tectonic activities, volcano eruptions and the others disaster management.

2. METHOD

2.1 Data

In the earlier 2019 a large scale aerial photogrammetric of the tsunami area was collected by the team member. We collected 105 aerial photos from the study area with the mean scale of 1:5000 and oriented to 3 GCPs on the site for photogrammetric processing as well as the evaluation of the derived DEMs. A typical feature, for instance, of mission plans for the research purpose is the large forward (60%) and cross (40-60%) overlap to compensate for aircraft instability. The mission management is to accommodate flightplans to the actual wind conditions of the mission area at the time of field survey. The flight path was predefined in GIS-like UAV control software and transferred to the UAV using a wireless connection.

For analysing the interferometric SAR we used SAR data derived from PALSAR-2 sensor and Images which L-band frequency characteristic on board from Advanced Land Observing Satellite (ALOS) with active microwave sensor to achieve cloud-free and day-and-night land observation. The dataset is composed of 2 SAR images, collected from 22 Sept 2014 and 9 Feb 2015 (Descending passes, HH polarization). In total, we selected 730 events with 3128 P- and 2050 S-phases. This dataset includes some deep focused events with depths of about 15 Km. The input data for the code are station coordinates and S-wave band arrival times of local earthquakes. The code can start performing calculations without using any a priori information on the sources. In this case, searching for the event locations starts from the center of the network or from the station with minimal travel time.

2.2 Photogrammetry Processing

The multiple aerial photos of the area were collected at a mean scale of 1:5000 and oriented to a GPS network of 3 ground control points (GCPs). Residual of bundle block adjustment on GCPs and tie points for outer orientation were on the order of few centimeter [Mora et al.,2003]. Digital photogrammetric techniques are currently the most interesting solution for the automatic generation of terrain models and orthophotos [Bitelli, G., et al 2004], which are highly important for the study of a disaster.

We used Agisoft Photoscan software for the image processing (alignment process, gradual selection, build dense cloud, build DEM, and Orthophoto) [Uysal, M. et al 2015 and Javernick, L. et al 2014]. Over 26 million georeferenced points were used in DEM generation process. Accuracy of the DEM was evaluated with 30 check points. In order to evaluate the accuracy's dependency on the number of GCPs used during indirect sensor orientation, six images of different acquisition altitudes were chosen to perform Aero-triangulation processing. During that test, the number of GCPs used during aerotriangulation varied from 3 to the maximum of GCPs that were visible in the image. For every number of control points the sensor orientation has been executed and the RMSE as well as the accuracy of the calculated orientation parameters were registered

2.3 Remote Sensing Processing

In this research we proposed InSAR method in the conventional single-interferogram approach, derives from two radar images of the same area acquired at different times to measure ground displacement [Veci, L., 2015]. The technique uses the phase difference of backscattered signals from the two acquisitions to measure differential motion in the Line Of Sight (LOS) direction include vertical and horizontal components. Differential-InSAR technique is a remote sensing method that allows to investigate single ground deformation event e.g. [Massonnet, D. and Rebaute, T., 1993]; [Peltzer, G. and Rosen, P., 1995]; [Rignot, E. and MacAyeal, D.R., 1998] on the earth surface with centimetre to millimetre accuracy.

We presented the interferometric analysis using snap software, a common architecture for all Sentinel Toolboxes is being jointly developed by Brockmann Consult, Array Systems computing and C-S called Sentinel Application Platform by ESA, (2016) to get interferogram and line of sight displacements the interferometric phase was unwrapped with the SNAPHU program. Measurements of local seismicity [Ibs-von Seht, M., 2008], electromagnetics, deformation analysis using InSAR, ground temperatures, meteorological parameters, sea level, chemical and physical parameters of fumarole gasses, and optical monitoring. On the other hand, the limitations of traditional D-InSAR technique is temporal and geometrical decorrelation, atmospheric distortions, imprecise terrain-models and uncertain the satellite orbits.

2.4 Run-up Model

The method used to model the Run-Up in this study is Regulation of the Minister of Public Works No.06/PRT/M/2009. Regarding the Ministerial Regulation No. 11 year 2016 of Ministry of Energy and Mineral Resources Indonesia (Kementerian ESDM) about the determination of Disaster-Prone Areas of Geological Hazard paragraph 1 point (2) and (6). Volcano hazard mitigation is an event how to reduce the risk of volcano hazard through the physical infrastructure nor establishing the awareness and ability for facing the the tsunami risk. Disaster-prone area of volcano hazard is the area which has inundated or identified as a potential hazard of tsunami with a direct nor indirect circumstances. In this paper we used vulnerability assessment to model disaster prone-areas. Vulnerability analysis of the elements at risk so as to assess their resistance to the impacts of the different anticipated physical effects. Vulnerability assessment in volcanic risk evalution (e.g. Aceves, Q., et al., 2007; and Dibben, C., et al., 1999) and the hazard event may influence the process of developing vulnerability for human assessment. From this, it is possible to assess the damage and determine the weak points in the regional system (Thierry, P., et al., 2008). The method of formulating the vulnerability assessment is Simple Additive Weight Method with the following equation:

$$V = a(A) + b(B) + c(C) + d(D) + ...$$

Where:

V = Vulnerability scale (Pairwise Comparison)

a, b, c, d = Value each criterion

A, B, C, D = Criterion assessment

The criterions are used number of population, time-series land surface, distance from the summit of volcano, lava flow. Population density was selected as the main indicator for social vulnerability. Disaster management tools are available to help minimize the risk and thereby the impact of a hazardous

3. RESULT AND DISCUSSION

3.1 DEM Generation

To maintain the feasibility of the project, not all the possible combinations of image pairs could be processed. Due to the fact that the UAV used for image acquisition didn't register the exterior orientation (EO) parameters for every captured image, it was necessary to perform a first sensor orientation for the whole dataset. To achieve this, the aerotriangulation was calculated using 3 GCPs for each of the 105 images. Next, in order to retain a wide variability of parameters like flying altitude, deviation from nadir-view, length of the photo base, etc., 97 image pairs were selected, covering the whole range of these variables. After this selection, the image pairs were processed in AgiSoft PhotoScan.

Figure 1. Images from aerial photo processing

In order to evaluate the accuracy's dependency on the number of GCPs used during indirect sensor orientation, six images of different acquisition altitudes were chosen to perform Aero-triangulation processing. During that test, the number of GCPs used during aerotriangulation. After aerial triangulation the multi-view images are reorganized to be divided automatically into basic units as the stereo pairs in traditional photogrammetry. Then the DSM is automatically generated by image matching and TIN interpolation within every unit. It need a little manual interaction operation to separate the points upon the building or lie down at grand for generation DEM. All units are link up to form fully coverage DEM. All the DEMs were saved in raster format with a ground sampling distance of 5.2 cm

3.2 Ground Deformation

In this study, we observed deformation in two objects, at the mainland of the island of Sumatra and the Anak Krakatoa volcano. Based on the processing at the Sumatera Island, it is seen that land subsidence occurs in the most coastal areas at the region of Liwa and Krui. Basically, we cannot clearly understand the impact of the 32-years of earthquake cycle of the ring of fire due to the limitations of the data being processed, by this study we only underlined that InSAR shows a range between -4 cm to 6 cm of vertical displacements in figure 3. This situation needs take a serious attention because these areas located in the hills along the coastline and Sumatran Fault.

For The RGB View can be useful for amplitude change detection. Regarding to ESA SNAP (2016) those images, we will see things that have changed in red or green and things that have not changed in yellow. It is also a visual indication that the coregistration has properly aligned both images. The resulting of RGB view should look mostly yellow. Poor registrations will have badly lined up terrain. The first result of interferograms as RGB could be allowed us to study interferometric SAR in volcano disaster.
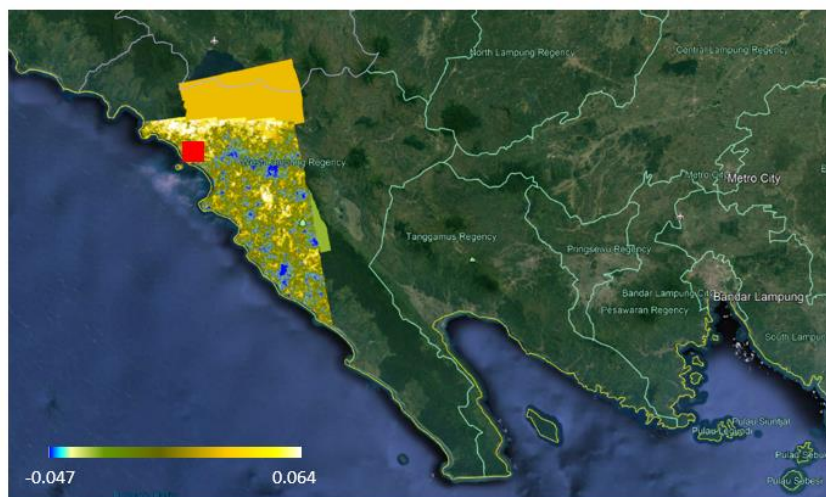
Figure 2. Differential InSAR result in vertical displacement at Southern Sumatera Island in metre. A red rectangular is a capital of Pesisir Barat Regency.
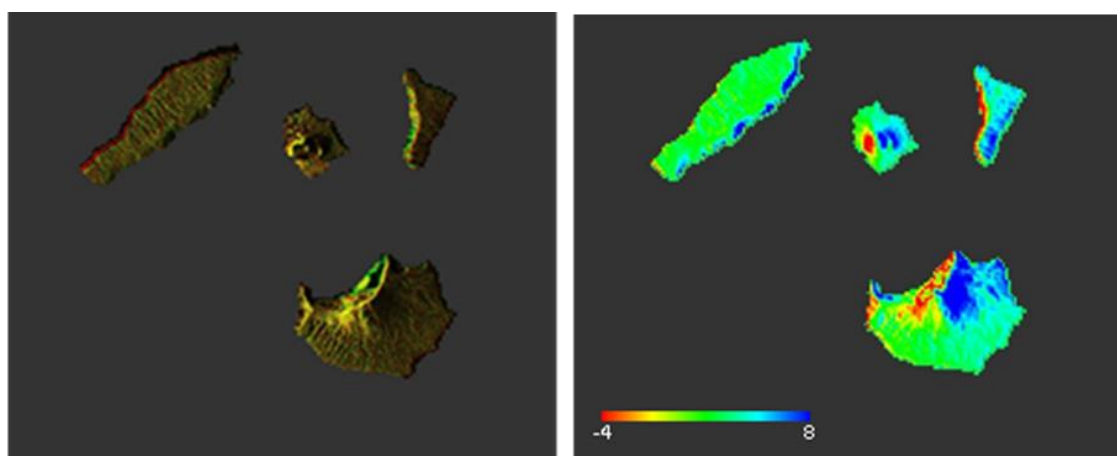
Figure 3. (a) RGB colour among slave and master image of SAR Data after coregistration (b) vertical displacement of Mt. Anak Krakatoa in centimetre

Due to periodic eruptions, the growth of the young cone becomes larger and conceals the old cone. The figure 2 shows the body over Mt. Anak Krakatoa becomes bigger, but there is no correlation among the complex of Krakatoa to explain the connectivity of each part about the complex of mountain growth. Based on CVGHM Indonesia, Anak Krakatoa is a typical cinder

cone with an approximate radius of 2 km. It rises up to 315 m above sea level and shows ongoing moderate activity, having grown at an average rate of ~8 cm/week over the last 80 years. In the area of Java and Sumatra, the northward subduction of the Indian oceanic plate under the Sunda block occurs at a rate of about 6.8–7.2 cm/yr [DeMets et al., 1990]. The displacement over Mt. Anak Krakatoa is relatively massive this could be affected by activity which dominated by continuing tremor vibration with maximum amplitude which tend to fluctuate with a potential to evoke phreatic eruptions and magmatic materials. The evidences can be taken to control potential geo disaster is possible to be obtained.

3.3 Model Run-Up and Vulnerability Area

The tsunami modeling based on historical records did not work well because of the uncertainty of tsunami generation [Mori, N. et al., 2011]. On the other hand, the vertical and horizontal distributions of run-up height are similar or more intense for the 2011 Tohoku tsunami that the 2004 Indian Ocean tsunami [e.g.,Karlssonet et al., 2009]. We modeled the run-up scenario based on DEM and ground deformation, landslide cause tsunami wave [Heidarzadeh, M. and Satake, K., 2015].

In this study, the height of a tsunami defined in maximum water level (hereinafter, inundation height); and run-up height. These are measured from sea level excluding astronomi-cal tide. Inundation height and run-up height were measured within a few centimeters accuracy from coastal. Run-up height was determined from the elevation, maximum landward extent of debris, distance and the area itself.
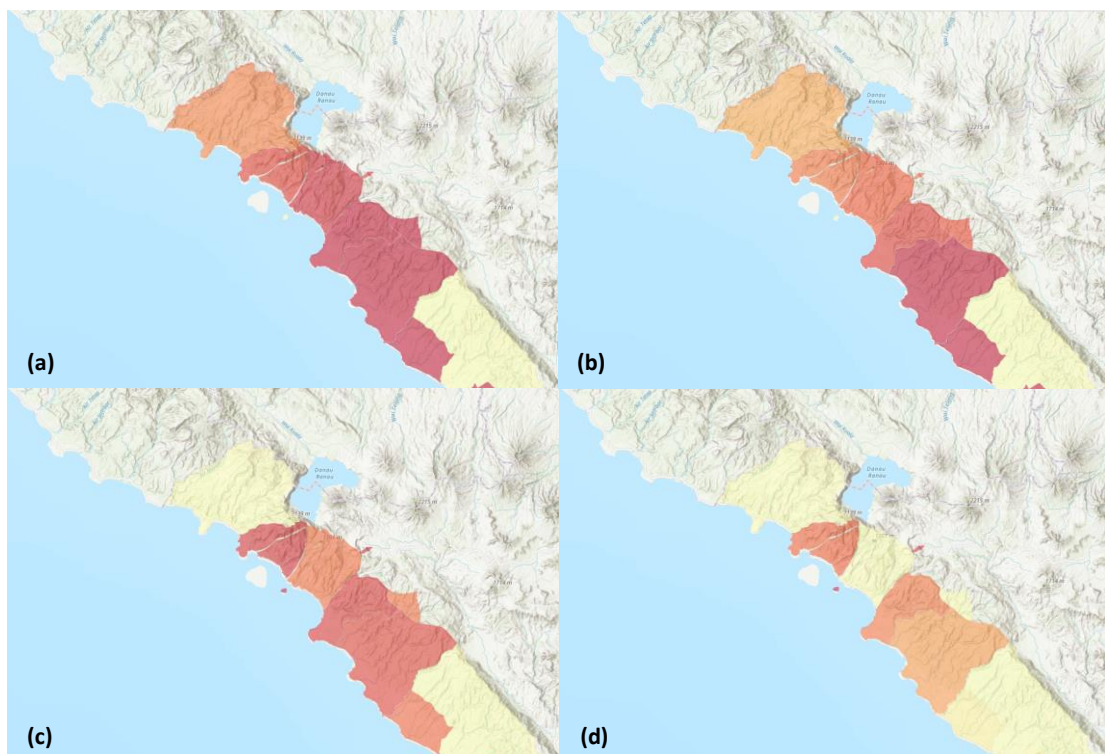
Figure 4. The tsunami model in the height of run-up (a) 45 meter;
(b) 30 meter; (c) 20 meter; and (d) 10 meter.

As an example Figure 4 shows local analysis of inundation height and run-up eight at Western Lampung bay. By using the high-density database of inundation and run-up information, local tsunami behavior can be assessed and analyzed in inundation areas. Furthermore, a notable feature of the data is that local inundation heights and run-up heights differed between neighboring locations. Sea walls, complex shading and diffraction by structures, and debris may play

important roles in changing local tsunami behavior. These macro roughness effects on inundation area are also difficult to consider by using the simple equation. The measurement data on inundation height and run-up height will be useful for investigating the effectiveness of tsunami protection during disaster risk preparedness.

4. CONCLUSION

Tsunami inundation heights were observed along Western Lampung stretch of the Sumatera coast from West Lampung to a part of South Lampung; tsunami inundation heights and run-up heights were modeled. The maximum run-up height in this event was similar to that in the Anak Krakatoa tsunami but the affected area was several times larger than the Anak Krakatoa tsunami. We modeled a maximum run-up heights of 45 m are distributed along the Western Lampung coast, in direct distance. For the further research, dynamic information about the tsunami such as velocity or the time course of the inundation process is required to understand this event. Social and historical recorded data will be helpful for estimating the necessary dynamic information.

Acknowledgements

References from Journals:

Aceves-Quesada, J.F., Díaz-Salgado, J. and López-Blanco, J., 2007. Vulnerability assessment in a volcanic risk evaluation in Central Mexico through a multi-criteria-GIS approach. Natural Hazards, 40(2), pp.339-356.

Bitelli, G., Dubbini, M. and Zanutta, A., 2004. Terrestrial laser scanning and digital photogrammetry techniques to monitor landslide bodies. *International Archives of Photogrammetry, Remote Sensing and Spatial Information Sciences*, *35*(B5), pp.246-251.

Dai, F., Dong, S., Kamat, V.R. and Lu, M., 2011. Photogrammetry assisted measurement of interstory drift for rapid post-disaster building damage reconnaissance. *Journal of Nondestructive Evaluation*, *30*(3), p.201.

DeMets, C., Gordon, R.G., Argus, D.F. and Stein, S., 1990. Current plate motions. *Geophysical journal international*, *101*(2), pp.425-478.

Dibben, C. and Chester, D.K., 1999. Human vulnerability in volcanic environments: the case of Furnas, Sao Miguel, Azores. *Journal of Volcanology and Geothermal Research*, *92*(1), pp.133-150.

Heidarzadeh, M. and Satake, K., 2015. New insights into the source of the Makran tsunami of 27 November 1945 from tsunami waveforms and coastal deformation data. *Pure and Applied Geophysics*, *172*(3-4), pp.621-640.

Ibs-von Seht, M., 2008. Detection and identification of seismic signals recorded at Krakatau volcano (Indonesia) using artificial neural networks. J. Volcanol. Geotherm. Res. 176, 448–456. doi:10.1016/j.jvolgeores.2008.04.015.

Javernick, L., Brasington, J. and Caruso, B., 2014. Modeling the topography of shallow braided rivers using Structure-from-Motion photogrammetry. *Geomorphology*, *213*, pp.166-182.

Karlsson, J. M., A. Skelton, M. Sanden, M. Ioualalen, N. Kaewbanjak,N. Pophet, J. Asavanant, and A. von Matern (2009), Reconstructions of the oastal impact of the 2004 Indian Ocean tsunami in the Khao Lak area,Thailand,J. Geophys. Res.,114, C10023, doi:10.1029/2009JC005516.

Lu, Z., Wicks Jr, C., Kwoun, O., Power, J.A. and Dzurisin, D., 2005. Surface deformation associated with the March 1996 earthquake swarm at Akutan Island, Alaska, revealed by C-band ERS and L-band JERS radar interferometry. *Canadian Journal of Remote Sensing*, *31*(1), pp.7-20

Massonnet, D. and Rabaute, T., 1993. Radar interferometry: limits and potential. IEEE Transactions on Geoscience and Remote Sensing, 31(2), pp.455-464

Mora, P., Baldi, P., Casula, G., Fabris, M., Ghirotti, M., Mazzini, E. and Pesci, A., 2003. Global Positioning Systems and digital photogrammetry for the monitoring of mass movements: application to the Ca'di Malta landslide (northern Apennines, Italy). *Engineering geology*, *68*(1-2), pp.103-121.

Mori, N., Takahashi, T., Yasuda, T. and Yanagisawa, H., 2011. Survey of 2011 Tohoku earthquake tsunami inundation and run-up. *Geophysical research letters*, *38*(7).

Peltzer, G. and Rosen, P., 1995. Surface displacement of the 17 May 1993 Eureka Valley, California, earthquake observed by SAR interferometry. Science, 268(5215), p.1333.

Rignot, E. and MacAyeal, D.R., 1998. Ice-shelf dynamics near the front of the Filchner—Ronne Ice Shelf, Antarctica, revealed by SAR interferometry. Journal of Glaciology, 44(147), pp.405-418.

Thierry, P., Stieltjes, L., Kouokam, E., Nguéya, P. and Salley, P.M., 2008. Multi-hazard risk mapping and assessment on an active volcano: the GRINP project at Mount Cameroon. *Natural Hazards*, *45*(3), pp.429-456.

Uysal, M., Toprak, A.S. and Polat, N., 2015. DEM generation with UAV Photogrammetry and accuracy analysis in Sahitler hill. *Measurement*, *73*, pp.539-543

Zaennudin, A., 2010. The characteristic of eruption of Indonesian active volcanoes in the last four decades, J. Lingkungan dan Bencana Geol, 1, pp.113-129.

References from Book
Veci, L., 2015 Interferometry Tutorial Copyright © 2015 Array Systems Computing Inc. http://www.array.ca/ http://step.esa.int